

# Flow behaviors of multi-scale bubbles with porous ceramic membrane distributors: Visualization and Modeling

Zhenli Xiang<sup>1</sup>, Chunyu Yin<sup>2</sup>, Dongchuang Wan<sup>2</sup>, Yebin Zhou<sup>2</sup>, Chaofan Ma<sup>2</sup>, Mengmeng Jiang<sup>2</sup>, Wei He<sup>2</sup>, Yi Liu<sup>1</sup>, Xiao-nian Li<sup>3</sup>, and Chunshan Lu<sup>1</sup>

<sup>1</sup>Zhejiang University of Technology

<sup>2</sup>Affiliation not available

<sup>3</sup>Institute of Industrial Catalysis

February 24, 2023

## Abstract

The distribution of gas-liquid two-phase flow is one of significant effects on heterogeneous catalytic reactions. Ceramic membrane gas distributors (CMGD) were applied in improving gas-liquid distribution, and flow behavior of gas as dispersed phase in liquid phase was visualized via high-speed photograph. The average diameters of multi-scale bubbles were measured and modeled ranging from  $10^{-5}$  to  $10^{-2}$  m. The coalescence and trajectory of bubbles during rising process were observed, and two typical trajectories straight and spiral types were tracked. In order to inhibit coalescence of bubbles during rising process, internals manufactured by 3D printing were installed in the channel of ceramic membrane. The average bubble size of CMGD decreases 12 % from 392 to 345  $\mu\text{m}$  compared to that of the original CMGD. The CMGD with internals enhances the heterogeneous catalytic reaction performance via providing large quantity of stabile multi-scale bubbles which could match the porous structure of catalyst.

## Flow behaviors of multi-scale bubbles with porous ceramic membrane distributors: Visualization and Modeling

Zhenli Xiang, Chunyu Yin, Dongchuang Wan, Yebin Zhou, Chaofan Ma, Mengmeng Jiang, Wei He, Yi Liu\*\*, Xiaonian li\*\*, Chunshan Lu\*

*State Key Laboratory Breeding Base of Green Chemistry Synthesis Technology, Zhejiang University of Technology, Hangzhou 310032, PR China.*

\* Corresponding author: [lcszjcn@zjut.edu.cn](mailto:lcszjcn@zjut.edu.cn);

\*\*Corresponding author: [yiliu@zjut.edu.cn](mailto:yiliu@zjut.edu.cn);

[xnli@zjut.edu.cn](mailto:xnli@zjut.edu.cn);

**KEYWORDS:** ceramic membrane, multi-scale bubbles, internals, bubble trajectory, coalescence

**Abstract:** The distribution of gas-liquid two-phase flow is one of significant effects on heterogeneous catalytic reactions. Ceramic membrane gas distributors (CMGD) were applied in improving gas-liquid distribution, and flow behavior of gas as dispersed phase in liquid phase was visualized via high-speed photograph. The average diameters of multi-scale bubbles were measured and modeled ranging from  $10^{-5}$  to  $10^{-2}$  m. The coalescence and trajectory of bubbles during rising process were observed, and two typical trajectories straight and spiral types were tracked. In order to inhibit coalescence of bubbles during rising process, internals manufactured by 3D printing were installed in the channel of ceramic membrane. The average bubble size of CMGD decreases 12% from 392 to 345  $\mu\text{m}$  compared to that of the original CMGD. The

CMGD with internals enhances the heterogeneous catalytic reaction performance via providing large quantity of stable multi-scale bubbles which could match the porous structure of catalyst.

## INTRODUCTION

Heterogeneous catalytic reaction is one of the most important reactions in the industrial production of fine chemicals.<sup>1-3</sup> The multiphase mass transfer efficiency can be intensified by stirring, reducing catalyst particle size, increasing reaction pressure and gas-liquid ratio.<sup>4-6</sup> In a fixed bed reactor, a continuous flow equipment, traditional gas-liquid distributors have many shortcomings, such as poor gas-liquid dispersion and unclear mixing, resulting in a low concentration of gas-phase reactants in the liquid phase, which seriously affects the performance of the multiphase catalytic reaction. In order to overcome this limitation, many techniques have been taken. Pickering emulsions,<sup>7</sup> microfluidic devices,<sup>8</sup> higee technology,<sup>9,10</sup> ultrasound method,<sup>11</sup> microwave method<sup>12</sup> and tube-in-tube technique<sup>13</sup> have been developed to boost interfacial area and gas adsorption. However, these methods require additional additives or complex equipment. It is crucial to develop a low-energy, continuous-feed gas distributor that strengthens gas-liquid mixing.

There are three approaches to enhance gas-liquid mass transfer: (a) increasing the liquid mass transfer coefficient; (b) increasing the saturated concentration of gas phase in liquid phase; (c) increasing the gas-liquid interfacial area.<sup>14</sup> The enhancement of mass transfer coefficient and saturated concentration requires high energy consumption, and the relatively easy method of increasing the gas-liquid interfacial area makes it the best way of gas-liquid mass transfer. The gas-liquid interfacial area can be increased by reducing the diameter of the bubbles in the gas-liquid system. Bubbles of millimeters and microns in size are capable of continuously produced by the micro-nano porous structure of ceramic membranes.<sup>15</sup> The gas-liquid two-phase interfacial area is elevated by increasing the gas holdup and reducing the size of the bubbles. Small size bubbles have a large specific surface area, which is beneficial to heighten the gas-liquid mass transfer rate. The microchannels can effectively reduce bubble size and have the advantages of uniform mixing, fast mixing rate and good stability, while the fluid cleanliness requirements are high and the pressure drop of the channel is relatively large due to the small mixing area.<sup>16-18</sup> Another method is membrane dispersion technology, which uses porous membrane materials as dispersion media to achieve micro-scale mixing. Compared to T- and Y-mixers, the porous structure of the ceramic membrane acts as a gas distributor, generating microbubbles in the liquid phase. Bubbles prepared through the nano-micro pores of ceramic membranes are typically several hundred micrometers in size. Micrometer-sized bubbles coalesce to form millimeter-sized bubbles in the rising process, which undoubtedly reduces the phase interfacial area with the liquid phase. The stability of bubble rising process deserves to be noted and the solutions should be presented.

In recent years, ceramic membranes have attracted more and more attention due to their excellent gas-liquid dispersed property. Khirani et al.<sup>16</sup> investigated the effects of different combinations of dispersed and continuous phases on microbubble generation, microbubble size proposing to the physicochemical properties of the two phases and the properties of the membrane surface. Chen et al.<sup>19-23</sup> evaluated the macroscopic dispersion of bubbles enhanced by membrane dispersion. In addition, they coupled the numerical simulation method of Navier-Stokes equation and Darcy equation to predict the gas permeation process in porous ceramic membranes. Zhang et al.<sup>24-26</sup> compared the effects of hydrophilic ceramic membranes and hydrophobic PTFE membranes, solvent type, and internals on bubble size. However, most works have focused on the structural parameters of ceramic membranes and the preparation of microbubbles. Very few reported shape and size changes of bubbles and the effects of trajectory on bubble stability during rising process.

In this work, a single-channel ceramic membrane was applied as a gas distributor, and high-speed photograph technology was used to investigate the effect of operating conditions on the gas-liquid two-phase flow pattern and bubble distribution, aiming to controllably prepare bubbles of corresponding sizes. Firstly, a CMGD was built to prepare micrometer-sized bubbles, and a high-speed photograph setup was constructed above the CMGD. Secondly, the effects of ceramic membrane length and gas pressure on bubble size were investigated. Subsequently, the bubble flow patterns were classified and the flow pattern transition line was obtained.

Finally, the effects of gas flow rate, liquid flow rate and rising distance on bubble size were discussed, and the modeling of bubble size was proposed and verified. In addition, visualization experiment also analyzed the coalescence process and motion trajectory of the bubbles, and installation of baffle-type internals influence the trajectory of bubbles, leading to inhibiting bubble coalescence and making the bubbles rise stably.

## EXPERIMENTAL SECTION

### 2.1 Materials and Setup

The average pore size of single channel ceramic membrane (Zhishen Fluid Membrane Separation Technology Operation Department, China) is  $0.2 \mu\text{m}$ . The inner and outer diameters are 8 mm and 12 mm separately. The ceramic membrane in the core of CMGD disperses the gas into micrometer-sized bubbles, and the schematic of the experimental setup is shown in Figure 1. The peristaltic pump and mass flow controller (MFC, D07-19B, Beijing Sevenstar Flow Co. Ltd.) are used to feed the two-phase fluids and control their flow rates. In the work, the volume flow rates of gas (nitrogen,  $\text{N}_2$ ) was varied from 5 ml/min to 50 ml/min by an MFC and the volume flow rates of deionized water (Reverse osmosis water purification equipment purchased from Sichuan Xixi Science and Technology Co., Ltd., China) was varied from 0.5 ml/min to 5 ml/min by a peristaltic pump (LM40B, Nanjing Runze Fluid Control Equipment Co., Ltd.). The visualization system was assembled by a high-speed camera (NPX-GS6500UM, Dongguan Qiansheng Electronic Technology Co., Ltd.) with a 12 mm macro len (NPX0412M14IR-2M, Dongguan Qiansheng Electronic Technology Co., Ltd.), a telecentric len of 110 mm object distance (Dongguan Qiansheng Electronic Technology Co., Ltd.), a quartz glass tube (outer diameter, 16 mm; inner diameter, 13 mm), and a LED light source (white light, 150 W). The rising dynamics of the bubbles were captured at 790 frames per second (fps) and 1 ms exposure time in a field of view of  $640 \times 480$  pixels. The camera position was set in front of the exit of the ceramic membrane to capture bubbles in the two-phase flow, and the camera was mounted on a slide to capture bubbles rising up to 5 cm and 10 cm. Additionally, internals with different numbers of baffles (as shown in Figure 2A-C) were designed using UG NX 12.0. The internals with a length of 10 cm were printed by a 3D printer (ANYCUBIC Photon Ultra) and placed in ceramic membrane channels to intensify the stability of bubbles.

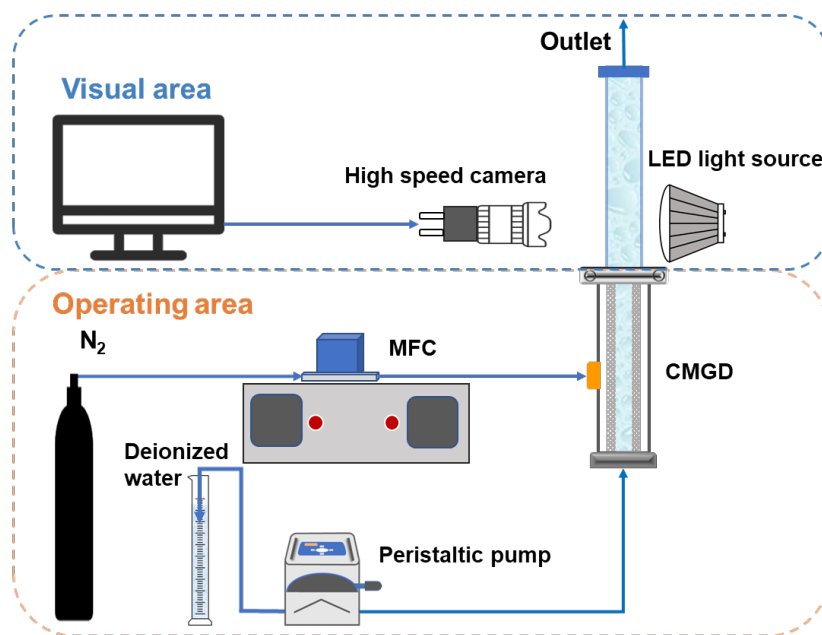


**FIGURE 1** The schematic of visual experimental apparatus with CMGD

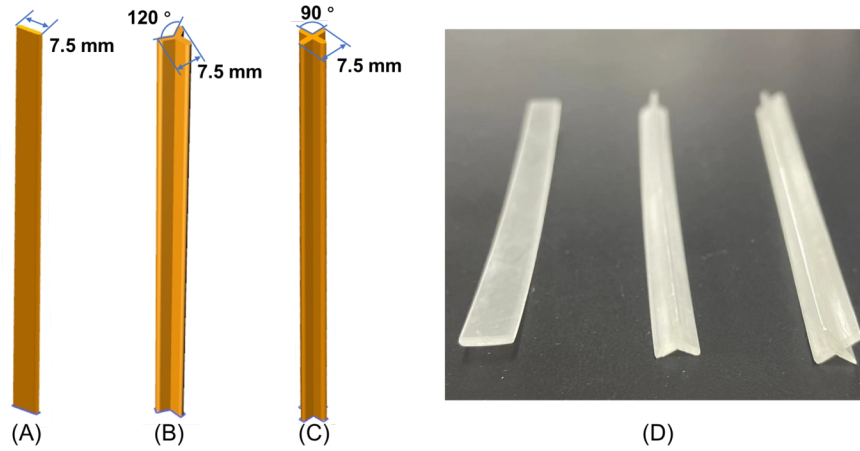


**FIGURE 2** 3D model of internals with (A) one-baffle, (B) Three-baffle, and (C) Four-baffle; (D) 3D printed internals based on 3D model

## 2.2 Image and Data Processing

All images were analyzed by Image J (version: 1.8.0) to determine the size and quantity of bubbles. The evaluation of the performance of the CMGD was based on the average diameter ( $d_{av}$ ) of bubbles. The bubble diameter was measured by the following steps: (1) setting scale, (2) selecting measurement area ( $15 \times 15$  mm), (3) calculating the equivalent diameter of bubbles. As shown in Figure 3A, the marked 4 chord lengths pass through the center of mass of the bubble as far as possible, and the final equivalent diameter of the bubble is the average of all chord lengths.<sup>27</sup> The diameter( $d_i$ ) of a single bubble is obtained by the above method, and the  $d_{av}$  of bubbles was calculated by eq (1):

$$d_{av} = \frac{1}{n} \sum_{i=1}^n d_i \quad (n > 300) \quad (1)$$

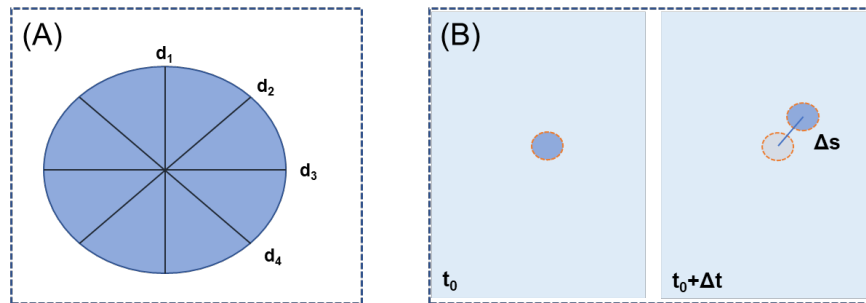


**FIGURE 3** Schematic diagram of (A) bubble equivalent diameter calculation and (B) bubble velocity calculation

Significance analysis was calculated by IBM SPSS Statistics 21.0. The rising behavior characteristics of bubbles was analyzed by kinovea (version:0.8.22). The rising trajectory of the bubble was observed by

tracking the path from image sequences. Since  $\Delta t$  (10 ms) is short enough and distance could be replaced by displacement, the velocity ( $v$ ) of bubble is calculated according to the time interval of two adjacent images and the straight-line distance of the center of mass of the bubble as illustrated in Figure 3B. The  $v$  was calculated by measuring the distance between the centroids of the fitted ellipse in the two successive images and the corresponding time difference from a known image capturing frame rate as follows:

$$v = \frac{\Delta \zeta}{\Delta t}$$

greek

(2)

The Weber ( $W$ ) number represents the ratio of inertia force to surface tension effect. The smaller the Weber number is, the more important the surface tension is. The calculation equation of  $W$  is as follows:

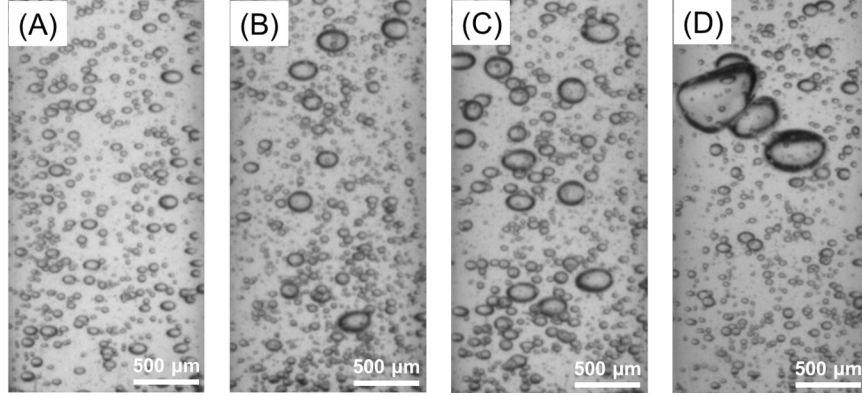
$$W = \frac{\rho v^2 l}{\sigma} \quad (3)$$

where  $\rho$  is the fluid density ( $\text{kg/m}^3$ ),  $v$  is the characteristic flow velocity ( $\text{m/s}$ ),  $l$  is the characteristic length ( $\text{m}$ ), here refers to the inner diameter of the ceramic membrane  $d$  ( $\text{m}$ ), and  $\sigma$  is the surface tension coefficient of the fluid ( $\text{N/m}$ ).

## RESULTS AND DISCUSSION

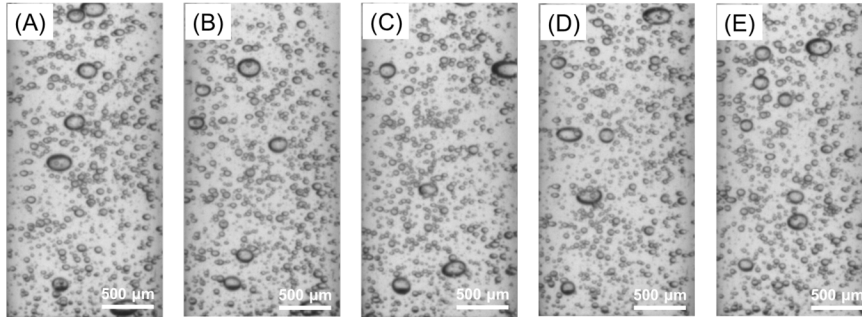
### 3.1 Effect of ceramic membrane length and gas pressure on bubbles size

Figure 4 shows typical images of bubbles generated by ceramic membranes with different lengths at a liquid flow rate of 1.0 ml/min and a gas flow rate of 10 ml/min. It can be seen that the distribution of bubbles generated by the ceramic membrane with 10 cm length is the most uniform, and the quantity of bubbles is larger than other length's membranes. Bubbles generated from a ceramic membrane with a length of 5 cm are also well distributed, while the small effective membrane pore area which is proportional to the length, leading to less quantity of bubbles than 10cm ceramic membrane. As the length of the ceramic membrane increased, the possibility of bubble coalescence increased during the rising process, resulting in larger size and less quantity of bubbles.<sup>16</sup> Figure 5 indicates that the average diameter of bubbles decreases first and then increases with the increase of the length of ceramic membrane. Under conditions that the length of the ceramic membrane was 10 cm, the average diameter of the bubbles was the smallest, only 320  $\mu\text{m}$ , which was smaller than other ceramic membranes. Figures 6 and 7 are performed to demonstrate that the changes of gas pressure in the range of 0.2-0.6 MPa have few effects on the flow pattern, distribution, and size of bubbles. In other words, when the gas feed at low pressure (no more than 0.6 MPa), the increase of gas pressure has no effect on the average diameter of bubbles. Results also illustrate that the CMGD does not require extra energy consumption as a green and high-performance gas distributor.



**FIGURE 4** Images of microbubbles formed at different lengths of ceramic membranes: (A) 5 cm, (B) 10 cm, (C) 15 cm, and (D) 20 cm. Liquid flow rate: 1.0 ml/min and gas flow rate: 10 ml/min

**FIGURE 5** Effects of lengths of ceramic membranes on the average bubble diameter



**FIGURE 6** Images of microbubbles formed at different pressures: (A) 0.2 MPa, (B) 0.3 MPa, (C) 0.4 MPa, (D) 0.5 MPa and (E) 0.6 MPa. Liquid flow rate: 1.0 ml/min and gas flow rate: 10 ml/min with 10 cm ceramic membrane

**FIGURE 7** Effect of gas pressure on the average bubble diameter. Liquid flow rate: 1.0 ml/min and gas flow rate: 10 ml/min with 10 cm ceramic membrane

### 3.2 Flow Pattern

The flow patterns of gas-liquid in ceramic membranes mainly include bubble flow and slug flow, as shown in Figure 8. It can be seen that the shape of the bubble is closely related to the gas flow and liquid flow. Therefore, a prediction model based on the critical point bubble for flow pattern is proposed as Eq. (4):

$$\begin{cases} Q_G = 45 - 26Q_L & (0 < Q_L < 1, 0 < Q_G < 20) & R^2 = 0.94857 & \text{bubble flow} \\ Q_G = 16.5 + 2.5Q_L & (Q_L \geq 1, Q_G \geq 20) & R^2 = 0.85714 & \text{slug flow} \end{cases} \quad (4)$$

When the liquid flow and gas flow are low, the gas phase is discontinuously distributed in the form of small bubbles in the liquid phase. The bubbles are spherical but the gas holdup is low, and the flow pattern at this time is mainly sparse bubble flow (Figure 9A). With the increase of gas flow, more small bubbles are generated and transferred to bubble flow (Figure 9B). As the gas flow rate continues to increase, the small bubbles gather and transform into large bubbles, which take on the shape of a convex front and a flat back,

with the flow pattern transforming into the slug flow in Figure 9C. It has been found large bubbles have a small phase interfacial area, which is not conducive to mass transfer.<sup>28</sup>

**FIGURE 8** Flow patterns with ceramic membrane of two phases. Liquid flow rate: 1.0 ml/min and gas flow rate: 10 ml/min with 10 cm ceramic membrane

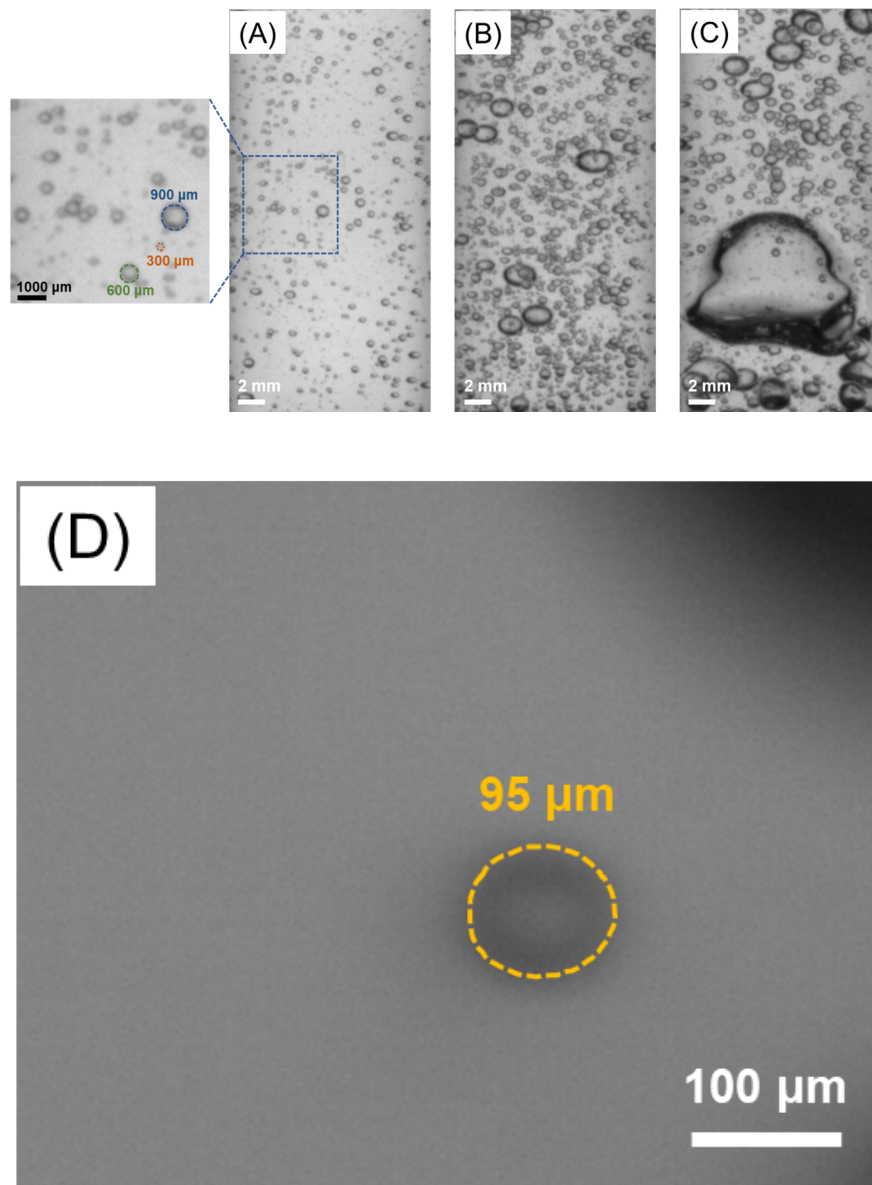


**FIGURE 9** Patterns of typical microbubbles formed by ceramic membrane: (A) sparse bubble flow, (B) dense bubble flow, (C) slug flow; (D) Micron bubble captured by a telecentric lens

The liquid among bubbles flows upwards, while the liquid layer between the bubbles and the pipe wall flows downwards slowly. Under the flow of slug flow, the bubbles gather into gas bombs, and the phase interfacial area between gas and liquid decreases. Therefore, the gas flow rate and liquid flow rate of the CMGD should be controlled as much as possible within the bubble flow range to obtain a high gas-liquid interfacial area.

### 3.3 Bubble Size

#### 3.3.1 Effect of Gas Flow Rate on Bubble Size

Figure 10 shows the effect of gas flow rate on  $d_{av}$ . Higher gas flow rates contribute to larger bubble sizes with  $d_{av}$  mainly in the 100 - 300  $\mu\text{m}$  range (Figure S3). With the increase of gas flow rate, the quantity of bubbles gradually increases, and  $d_{av}$  also increases. The increase of quantity of bubbles raises the collision frequency of bubbles. Thus, the coalescence of bubbles makes  $d_{av}$  increase, and the corresponding quantity of bubbles declines. In terms of gas flow rate is 10 ml/min, the largest quantity of bubbles ( $\sim 500$ ) is observed.

**Figure 10** Effects of gas flow rate on bubble sizes ( $d_{av}$ ) and quantity at a liquid flow rate of 1.0 ml/min with 10 cm ceramic membrane

#### 3.3.2 Effect of Liquid Flow Rate on Bubble Size

Figure 11 conveys the variation of bubble size and quantity with liquid flow rate. The increase of liquid flow rate reduces the residence time of bubbles, resulting in a drop in quantity of bubbles. The  $d_{av}$  slightly changes from 330 to 340  $\mu\text{m}$  at the liquid flow rate of 1-3 ml/min, and the quantity of bubbles decreased 16%. As the liquid flow rate is greater than 3 ml/min, the  $d_{av}$  augment to 388  $\mu\text{m}$ , and the quantity of bubbles decreased to 355 at 4 ml/min of liquid flow rate. With the increasement of liquid flow rate, the shear force of the liquid becomes larger, so that the drag force of the bubble during the growth process also gets larger. The unshedding bubble will coalesce with the adjacent bubble, and the bubble would start to expand. Since a growth of liquid flow rate made the bubble collision frequency and velocity ascend, the bubbles tended to coalesce, resulting in the increase of bubble size and the decrease of bubble quantity.

**FIGURE 11** Effects of liquid flow rate on bubble sizes ( $d_{av}$ ) and quantity at a gas flow rate of 10 ml/min with 10 cm ceramic membrane

#### 3.3.3 Effect of Rising Distance on Bubble Size

Figure 12 implies the variation of the  $d_{av}$  and bubble quantity with the rising distance of bubbles. In the range of 0-10 cm from CMGD, the  $d_{av}$  gradually rise and the quantity of bubbles decreased with the increasement of rising distance. Because the bubbles in the water are impacted by the internal pressure of the water, and they are under less pressure as rising, resulting in a larger bubble volume. The large bubble disturbs the flow field more, attracting more small bubbles around them. Moreover, small bubbles coalesce when they are close to large bubbles. After the coalescence, the volume of large bubbles becomes larger, which will exert more influence on the surrounding flow field and other small bubbles. As a result, the bubble size magnifies while the quantity decreases with the increase of bubble rising distance. This provides a reference for the filling position of the catalyst for the gas-liquid-solid three-phase reaction in the fixed bed, that is, as close as possible to the exit of the ceramic membrane distributor, in order to avoid the influence of the coalescence of bubbles on the gas-liquid mass transfer.

**FIGURE 12** Effects of rising distance on bubble sizes ( $d_{av}$ ) and quantity at a gas flow rate of 10 ml/min with 10 cm ceramic membrane

#### 3.3.4 Modeling of bubble average diameter

According to the Weber number and the flow ratio of the gas phase ( $Q_G$ ) to the liquid phase ( $Q_L$ ), a prediction model of the bubble size is proposed:

$$\frac{d_{av}}{d_m} = k \times W^a \times \left( \frac{Q_G}{Q_L} \right)^b \quad (5)$$

After fitting the experimental data, the equation for the bubble size of the dispersed gas generated by the

ceramic membrane is obtained:

$$\frac{d_{av}}{d_m} = 6818.48 \times W^{0.11675} \times \left( \frac{Q_G}{Q_L} \right)^{-0.00357} \quad (6)$$

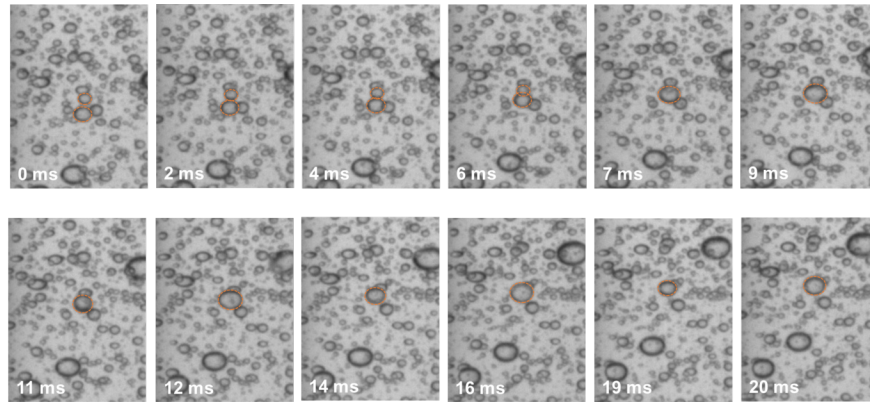
Figure 13 suggests that the theoretical data is basically consistent with the experimental data, and the relative error is 30% positive deviation and 15% negative deviation. In fact, the size of the bubbles is also affected by many factors, such as the wettability of the membrane, the pore size of the membrane, and the physical properties of the liquid. The next research will consider building a more complete model.

**FIGURE 13** Prediction and verification of average diameter model of microbubbles produced by ceramic membrane

### 3.4 Bubble Behavior Characteristic

#### 3.4.1 Coalescence

The change in bubble size distribution may be related to the change of bubble coalescence and fragmentation. Therefore, the investigation of bubble coalescence is of great significance for the stable rising of bubbles. Figure 14 shows typical coalescence process of two bubbles. In that case a bubble accelerated to impact a previous bubble, two bubbles will experience (1) bubble collision ; (2) formation and drainage of liquid film between bubbles ; (3) rupture of the liquid film until the three stages of coalescence.<sup>29</sup> Due to the fast velocity of the large bubble below, it catches up with a neighboring small bubble above at 2 ms, while the two bubbles deform (gourd shape) at 4 ms. A large bubble catches up with a neighboring small bubble above at 2 ms due to the fast velocity of large bubble below, and the two bubbles deform to a gourd shape at 4 ms. The liquid between the two bubbles is squeezed out and formed a thin liquid film. The two bubbles break the liquid film limit at 7ms to complete the coalescing. The coalesced large bubbles are continuously deformed under the action of surface tension and inertial force.<sup>30</sup>



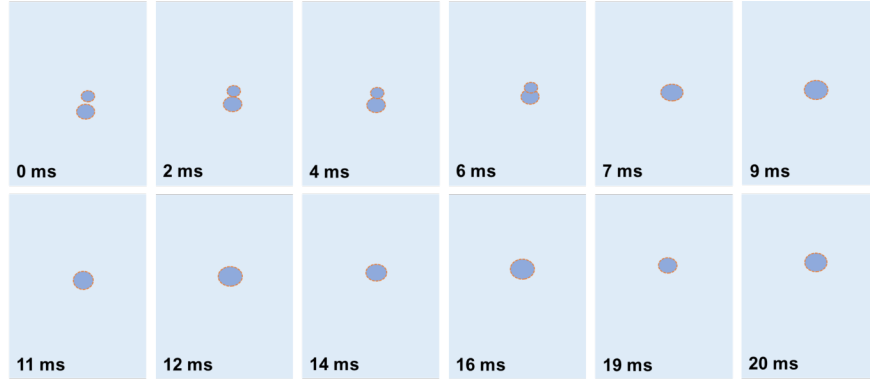


**FIGURE 14** Bubbles coalescence process images and schematic diagram

### 3.4.2 Trajectory

Figure 15 shows bubble trajectory with different diameters. When the diameter of bubble is greater than  $1000\ \mu\text{m}$ , the trajectory is spirally rising, and the residence time is short. While the trajectory is almost straight up at a diameter less than  $1000\ \mu\text{m}$ , and the residence time is longer. The bubbles show morphological changes with different oscillation amplitudes during the ascent. Under the action of buoyancy, the bubbles begin to gradually accelerate to the final velocity state. Affected by resistance and buoyancy, there is a large pressure difference between the upper and lower parts of the bubbles.<sup>31</sup> The bubbles are deformed by the pressure difference. The larger the bubble diameter, the more obvious the deformation. This reveals that the smaller diameter bubbles are more stable. As the diameter of the bubble grows, the effect of liquid shear-induced lift is more obvious, and the lateral movement of the bubble is more significant, so that the movement trajectory of the bubble is a spiral upward.<sup>28,32</sup> As the diameter of the bubble decreases, the response of the bubble to the velocity gradient in the channel gradually decreases, and the upward trajectory is hardly affected. Figure 16 indicates the rising velocity of bubbles varies with different diameters. The velocity of the bubbles with a diameter of  $1.3\ \text{mm}$  fluctuates between  $0.15$  and  $0.27\ \text{m/s}$ . The inflection point of the velocity variation corresponds to the turning point when the bubbles spiral upward, and the rising velocity of the bubbles tends to decrease in general. The velocity of the bubble with a diameter of  $0.56\ \text{mm}$  fluctuates in the range of  $0.04$ - $0.12\ \text{m/s}$ , which corresponds to a nearly straight line of its upward trajectory. The results demonstrate that bubbles with small diameters are more stable with slow rising velocity, and the residence time in the liquid phase is longer, which is consistent with the rising trajectory of the previous bubbles.

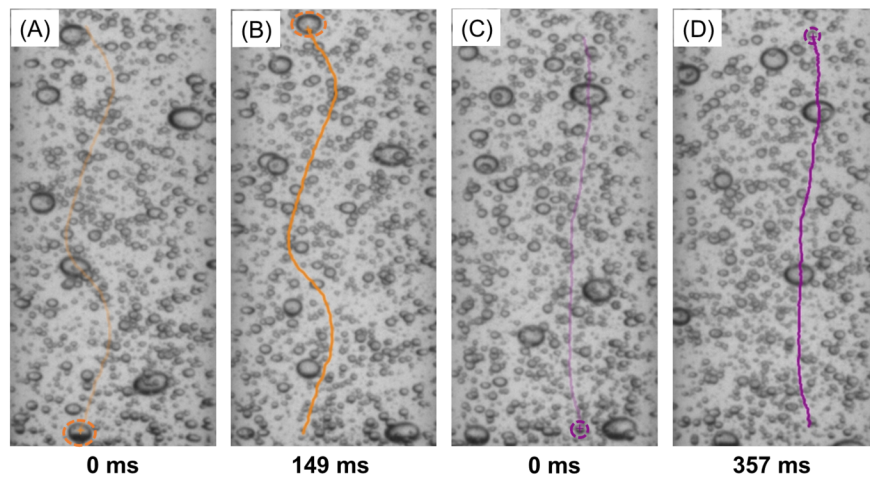


**FIGURE 15** (A) start and (B) end of the trajectory of the bubble with a diameter greater than  $1000\ \mu\text{m}$ ; (C) start and (D) end of the trajectory of the bubble with a diameter less than  $1000\ \mu\text{m}$ . Liquid flow rate:  $1.0\ \text{ml/min}$  and gas flow rate:  $10\ \text{ml/min}$  with  $10\ \text{cm}$  ceramic membrane

**FIGURE 16** The rising velocities of bubbles with  $1.3\ \text{mm}$  and  $0.56\ \text{mm}$  diameters. Liquid flow rate:  $1.0\ \text{ml/min}$  and gas flow rate:  $10\ \text{ml/min}$  with  $10\ \text{cm}$  ceramic membrane

### 3.5 Intensification of bubble stability by internals

The control of bubble trajectory contributes to the regulation of bubble coalescence. After the installation of internals with different numbers of baffles, the average diameter of the bubbles is effectively controlled as the rising height increases. The collision frequency between bubbles is reduced by installing internals inside the ceramic membrane, thereby inhibiting the coalescence of bubbles. Especially when three-baffle and four-baffle internals are installed, the bubble sizes grow slightly during the rising process (Figure 17). The internals impede the radial migration of the bubbles, reducing the collision frequency and the possibility of coalescence, allowing for a steady rise and keeping the size around  $350\ \mu\text{m}$ . Subsequently, the trajectory of the bubble was tracked. The results suggest that the spiral rising characteristics of large diameter bubbles are weakened (Figure 18). The velocity of bubbles with a diameter of  $1.2\text{-}1.4\ \text{mm}$  after installing the internals is analyzed. The velocity varies slightly in the range of  $0.12\text{-}0.2\ \text{m/s}$  as shown in Figure 19, which is slower than the bubble velocity of  $1.3\ \text{mm}$  diameter without internals. This indicated that the baffle internals could maintain the stability of bubbles by reducing the bubble rising velocity.

**FIGURE 17** Effect of baffle number of internals on bubble size at rising distance of  $0\ \text{cm}$ ,  $5\ \text{cm}$  and  $10\ \text{cm}$ . Liquid flow rate:  $1.0\ \text{ml/min}$  and gas flow rate:  $5\ \text{ml/min}$  with  $10\ \text{cm}$  ceramic membrane

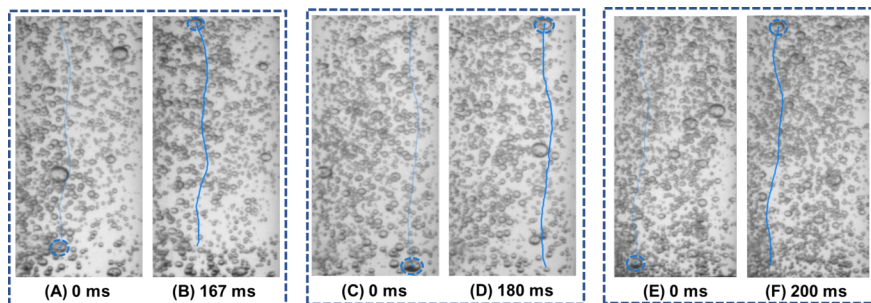


**FIGURE 18** Bubble trajectory with different number baffles: (A) and (B) one-baffle; (C) and (D) three-baffle; (E) and (F) four-baffle. Liquid flow rate:  $1.0\ \text{ml/min}$  and gas flow rate:  $5\ \text{ml/min}$  with  $10\ \text{cm}$  ceramic membrane

**FIGURE 19** The rising velocities of bubbles with  $1.2\text{-}1.4\ \text{mm}$  diameters in different number baffles. Liquid flow rate:  $1.0\ \text{ml/min}$  and gas flow rate:  $5\ \text{ml/min}$  with  $10\ \text{cm}$  ceramic membrane

## DATA AVAILABILITY AND REPRODUCIBILITY STATEMENT

The data that support the findings of this study are available from the corresponding author upon reasonable request. Source data are provided with this article. More than three independent replicate experiments were performed and the reproducibility of this research is good.

The bubble diameter distributions in Figures 10-12 are listed in Figures S1-3 of the supplementary material.

All videos are included in video.zip. The videos of bubble flow pattern in Figure 9 are Sparse bubble flow.avi, Dense bubble flow.avi, and Slug flow.avi in supplementary material. Videos of Coalescence.avi, Bubble trajectory-spiral.avi, and Bubble trajectory-straight.avi are bubble coalescence and trajectory, which are related to Figures 14 and 15.

Error bars in Figures 5, 7, 10, 11, and 12 show the spread of data observed in triplicate measurements. The air tightness of CMGD should be tested before the experiment in order to ensure the reliability and reproducibility of the experiment.

## CONCLUSIONS

In order to intensify the mass transfer for gas-liquid-solid reaction in fixed bed, CMGD was applied to disperse gas into a large quantity of multi-scale bubbles in liquid phase, increasing the gas-liquid interfacial area to improve the mass transfer efficiency. The effects of gas-liquid flow rate and rising height on bubble size were investigated. The results show that the  $d_{av}$  is ranging from 330 to 345  $\mu\text{m}$  and the quantity of bubbles is 500 under the optimal conditions of 10 cm ceramic membrane, gas flow rate of 10 ml/min, liquid flow rate of 1 ml/min. A large number of bubbles will coalesce in ceramic membrane channel and rising process, which is contrary to the strategy of increasing the two-phase boundary area. The ceramic membrane channel was divided into several channels by installing baffle-type internals, consequently reducing the radial migration between bubbles and significantly inhibiting the coalescence of bubbles. This work revealed the influence of operating conditions and internals on bubble size in CMGD, and discussed the deformation, coalescence, trajectory and velocity of multi scale bubbles, contributing to gas-liquid dispersion, enhancement of mass transfer efficiency and improvement of heterogeneous catalytic reaction performance.

## AUTHOR CONTRIBUTIONS

**Zhenli Xiang** : Formal analysis (equal); investigation (lead); methodology (equal); software (equal); visualization (equal); writing – original draft (lead). **Chunyu Yin** : Data curation (equal); investigation (equal). **Dongchuang Wan** : Data curation (equal); software (equal). **Yebin Zhou** : Conceptualization (equal); visualization (equal). **Chaofan Ma** : Investigation (supporting); methodology (equal). **Mengmeng Jiang** : Data curation (supporting); formal analysis (supporting). **Wei He** : Data curation (supporting); formal analysis (supporting). **Yi Liu**: Conceptualization (equal); data curation (equal); supervision (equal) writing – review & editing (equal). **Xiao-nian Li**: Writing – review & editing (equal). **Chunshan Lu** : Resources (lead); supervision (equal); writing – review & editing (lead).

## ACKNOWLEDGMENTS

This work was supported by the National Natural Science Foundation of China (No. 21978265, 22078302 and 22208301), the Key Program of the National Natural Science Foundation of China (No. U20A20119), and the Zhejiang Key Research and Development Program (NO. 2021C01081). The authors also gratefully acknowledge the financial support from the State Key Laboratory of Green Chemistry Synthesis Technology (GCST-20200006).

## REFERENCES

1. Alig L, Fritz M, Schneider S. First-Row Transition Metal (De)Hydrogenation Catalysis Based On Functional Pincer Ligands. *Chemical Reviews*. 2019;119(4):2681-2751.

2. Formenti D, Ferretti F, Scharnagl FK, Beller M. Reduction of Nitro Compounds Using 3d-Non-Noble Metal Catalysts. *Chemical Reviews*.2019;119(4):2611-2680.
3. Meemken F, Baiker A. Recent Progress in Heterogeneous Asymmetric Hydrogenation of C-O and C-C Bonds on Supported Noble Metal Catalysts.*Chemical Reviews*. 2017;117(17):11522-11569.
4. Kang P, Zhang S, Meyer TJ, Brookhart M. Rapid Selective Electrocatalytic Reduction of Carbon Dioxide to Formate by an Iridium Pincer Catalyst Immobilized on Carbon Nanotube Electrodes.*Angewandte Chemie International Edition*. 2014;53(33):8709-8713.
5. Zhang J, Rao C, Peng H, et al. Enhanced toluene combustion performance over Pt loaded hierarchical porous MOR zeolite. *Chem. Eng. J*. 2018;334:10-18.
6. Li W-L, Gao X-Y, Ouyang Y, et al. CFD Analysis of Gas Flow Characteristics and Residence Time Distribution in a Rotating Spherical Packing Bed. *Ind. Eng. Chem. Res*. 2019;58(47):21717-21729.
7. Yu Y, Fu L, Zhang F, Zhou T, Yang H. Pickering-Emulsion Inversion Strategy for Separating and Recycling Nanoparticle Catalysts.*ChemPhysChem*. 2014;15(5):841-848.
8. Günther A, Khan SA, Thalmann M, Trachsel F, Jensen KF. Transport and reaction in microscale segmented gas-liquid flow. *Lab on a Chip*.2004;4(4):278-286.
9. Zheng X-H, Chu G-W, Kong D-J, et al. Mass transfer intensification in a rotating packed bed with surface-modified nickel foam packing. *Chemical Engineering Journal*. 2016;285:236-242.
10. Chen Q-Y, Chu G-W, Luo Y, et al. Polytetrafluoroethylene Wire Mesh Packing in a Rotating Packed Bed: Mass-Transfer Studies.*Industrial & Engineering Chemistry Research*.2016;55(44):11606-11613.
11. Machado IV, dos Santos JRN, Januario MAP, Corrêa AG. Greener organic synthetic methods: Sonochemistry and heterogeneous catalysis promoted multicomponent reactions. *Ultrasonics Sonochemistry*.2021;78:105704.
12. Goyal H, Chen T-Y, Chen W, Vlachos DG. A review of microwave-assisted process intensified multiphase reactors.*Chemical Engineering Journal*. 2022;430:133183.
13. Kobayashi J, Mori Y, Okamoto K, et al. A Microfluidic Device for Conducting Gas-Liquid-Solid Hydrogenation Reactions. *Science*.2004;304(5675):1305-1308.
14. Ansari M, Bokhari HH, Turney DE. Energy efficiency and performance of bubble generating systems. *Chemical Engineering and Processing - Process Intensification*. 2018;125:44-55.
15. Hartman RL, Naber JR, Zaborenko N, Buchwald SL, Jensen KF. Overcoming the Challenges of Solid Bridging and Constriction during Pd-Catalyzed C-N Bond Formation in Microreactors. *Organic Process Research & Development*. 2010;14(6):1347-1357.
16. Khirani S, Kunwapanitchakul P, Augier F, Guigui C, Guiraud P, Hebrard G. Microbubble Generation through Porous Membrane under Aqueous or Organic Liquid Shear Flow. *Industrial & Engineering Chemistry Research*. 2012;51(4):1997-2009.
17. Zhao Y, Yao C, Chen G, Yuan Q. Highly efficient synthesis of cyclic carbonate with CO<sub>2</sub> catalyzed by ionic liquid in a microreactor.*Green Chemistry*. 2013;15(2):446-452.
18. Chen Y, Zhao Y, Han M, Ye C, Dang M, Chen G. Safe, efficient and selective synthesis of dinitro herbicides via a multifunctional continuous-flow microreactor: one-step dinitration with nitric acid as agent. *Green Chem*. 2013;15(1):91-94.
19. Li X, Liu Y, Jiang H, Chen R. Computational Fluid Dynamics Simulation of a Novel Membrane Distributor of Bubble Columns for Generating Microbubbles. *Industrial & Engineering Chemistry Research*. 2019;58(2):1087-1094.

20. Liu Y, Han Y, Li X, Jiang H, Chen R. Controlling microbubbles in alcohol solutions by using a multi-channel ceramic membrane distributor. *Journal of Chemical Technology & Biotechnology*. 2018;93(8):2456-2463.
21. Liu Y, Han Y, Li X, Jiang H, Chen R. Efficient Control of Microbubble Properties by Alcohol Shear Flows in Ceramic Membrane Channels. *Chemical Engineering & Technology*. 2018;41(1):168-174.
22. Han Y, Liu Y, Jiang H, Xing W, Chen R. Large scale preparation of microbubbles by multi-channel ceramic membranes: Hydrodynamics and mass transfer characteristics. *The Canadian Journal of Chemical Engineering*. 2017;95(11):2176-2185.
23. Hou M, Jiang H, Liu Y, Chen C, Xing W, Chen R. Membrane Based Gas-Liquid Dispersion Integrated in Fixed-Bed Reactor: A Highly Efficient Technology for Heterogeneous Catalysis. *Industrial & Engineering Chemistry Research*. 2018;57(1):158-168.
24. Xie B, Zhou C, Chen J, Huang X, Zhang J. Preparation of microbubbles with the generation of Dean vortices in a porous membrane. *Chemical Engineering Science*. 2022;247:117105.
25. Xie BQ, Zhou CJ, Sang L, Ma XD, Zhang JS. Preparation and characterization of microbubbles with a porous ceramic membrane. *Chemical Engineering and Processing - Process Intensification*. 2021;159:108213.
26. Xie B, Zhou C, Huang X, Chen J, Ma X, Zhang J. Microbubble Generation in Organic Solvents by Porous Membranes with Different Membrane Wettabilities. *Industrial & Engineering Chemistry Research*. 2021;60(23):8579-8587.
27. Shuai Y, Guo X, Wang H, et al. Characterization of the bubble swarm trajectory in a jet bubbling reactor. *AIChE Journal*. 2019;65(5):e16565.
28. Zeng W, Jia C, Luo H, Yang G, Yang G, Zhang Z. Microbubble-Dominated Mass Transfer Intensification in the Process of Ammonia-Based Flue Gas Desulfurization. *Industrial & Engineering Chemistry Research*. 2020;59(44):19781-19792.
29. Browne C, Tabor RF, Chan DYC, Dagastine RR, Ashokkumar M, Grieser F. Bubble Coalescence during Acoustic Cavitation in Aqueous Electrolyte Solutions. *Langmuir*. 2011;27(19):12025-12032.
30. Wang H, Zhang Z-y, Yang Y-m, Zhang H-s. Surface Tension Effects on the Behavior of Two Rising Bubbles. *Journal of Hydrodynamics*. 2011;23(2):135-144.
31. Li W, Jiao S, Tang K, Yang Y, Qu W, Chai X. Experimental Investigation on Characteristic of Single Bubble Motion in Stagnant Water. *Atom. Energy Sci. Technol.* 2020;54(09):1652-1659.
32. Yang B, Jafarian M, Freidoonimehr N, Arjomandi M. Trajectory of a spherical bubble rising in a fully developed laminar flow. *International Journal of Multiphase Flow*. 2022;157:104250.

## SUPPORTING INFORMATION

Additional supporting information may be found in the online version of the article at the publisher's website.